Magic-Sized Diamond Nanocrystals

I. B. Altfeder,[1,2] J. J. Hu,[1] A. A. Voevodin,[1] and J. Krim[2]

[1]*Materials and Manufacturing Directorate, Air Force Research Laboratory, RXBT, Wright-Patterson Air Force Base, Ohio, 45433, USA*

[2]*Physics Department, North Carolina State University, Raleigh, North Carolina, 27695, USA*

(Received 12 December 2008; published 2 April 2009)

The 2D structural transformation of a heavily boron-doped diamond surface has been revealed using scanning tunneling microscopy (STM). We found that at boron densities above the metal-insulator transition the diamond surface is comprised of spatially ordered magic-sized nanocrystals. The development of quantized electron gas inside these nanocrystals is directly confirmed by STM observation of standing electron waves. The experimental comparison of metallic and insulating diamond reveals the existence of the Fermi-sea-induced quantum selection rules for the self-assembly of nanostructures.

DOI: 10.1103/PhysRevLett.102.136104 PACS numbers: 68.65.−k, 68.37.Ef, 71.30.+h, 73.22.−f

The interplay of structural and electronic properties of materials represents one of the core problems of condensed matter physics. In nanoscale systems, this interplay often manifests itself as a competition between quantum effects, which control the electronic properties of nanostructures [1–6], and classical effects of atomic diffusion, which determine their growth and morphology [7–9]. The existence of unusual quantum selection rules, the quantum ''electronic growth'', affecting the size distribution of metallic nanostructures has been discovered in recent years [1,2,4–6]. According to this concept, the electron de Broglie wavelength controls the geometry of nanostructures and establishes the preferred size. The hypothesis of electronic growth had been already confirmed by observation of ''magic'' heights in thin metal films [2,4–6], and observation of magic-sized 2D molecular self-assembly on Cu(111) surface [10].

Diamond and diamond nanostructures represent very interesting and rich model object for structure-property relationship studies at nanometer scale. Although in its pure form diamond is known to be an insulator with a band gap of 5.5 eV, upon heavy boron-doping this material becomes a metal and at low temperatures even a superconductor [11–15]. Indeed, despite large electronic activation energy of boron atoms in diamond (373 meV), broadening of the impurity level at high dopant densities causes its overlap with diamond valence band edge followed by the insulator-to-metal transition. A size-dependent insulator-to-metal transition in diamond at high nitrogen doping was also experimentally observed and theoretically explained [16]. Thin films of diamond microcrystals and nanoparticles, both insulating and metallic, can be synthesized on a variety of solid substrates using the recently developed chemical vapor deposition (CVD) technique [17–21]. Because this technique combines the growth and the doping of nanostructures in the single deposition process, the influence of quantum electronic effects on the growth dynamics here can be directly studied. Previous scanning tunneling microscopy (STM) studies of this material had been focused on (2×1) dimer reconstruction [22], emission properties [23], and low-temperature superconducting properties [24,25].

In this Letter, we report the first STM observation of the quantum size-effect in boron-doped diamond. We found that at the surfaces of CVD-grown diamond films, the boron induced insulator-to-metal transition facilitates the self-assembly of spatially ordered magic-sized nanocrystals. We suggest that the development of this 2D superstructure is caused by the Fermi-sea-induced quantum electronic growth mechanism.

For this study, we used 2 μm thickness boron-free and boron-doped diamond films on silicon synthesized by Advanced Diamond Technologies, Inc. The samples were grown under similar conditions. The nominal impurity concentration in B-doped samples was 10^{20} cm^{-3}. The samples have been characterized using scanning electron microscopy (SEM) and variable-temperature ultra high vacuum STM (UHV300 from RHK Technology, Inc.).

The STM measurements on boron-doped samples were performed at room temperature. In Fig. 1 we show the large-scale STM and SEM (see the inset) images of boron-doped diamond films, whose surface structure was the main target of this work. On both images one can easily see large diamond grains whose sizes range from 0.2 to 1.0 μm, in close agreement with earlier published structural studies [26,27].

At the next stage of experiments, the STM tip was positioned on top of the individual diamond microcrystal. The flat facets of diamond microcrystals that were selected for our measurements exhibited modest tilt, which was typically $\leq 30°$ and could be electronically compensated during STM data acquisition. In Figs. 2(a) and 2(b) we show the typical STM images obtained on top surface of diamond microcrystals. The images are comprised of periodically ordered parallelogram-shaped grains. The existence of the two-dimensional order in these images is also

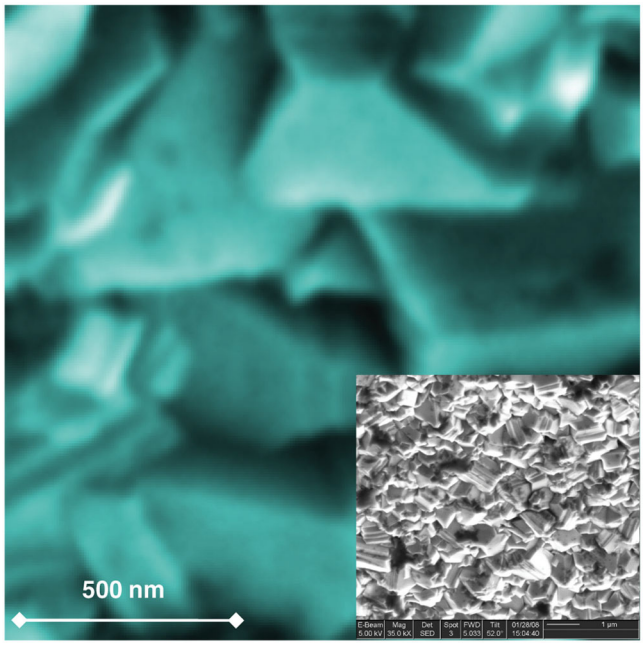

FIG. 1 (color). Boron-doped diamond microcrystals observed by STM at room temperature. The image sizes are 1.5×1.5 μm. The image was obtained using tunneling current $I = 0.1$ nA and tip bias $V = 1200$ mV. Inset: 7.3×6.3 μm SEM image of boron-doped diamond sample.

confirmed in the 2D STM Fourier transform shown in Fig. 2(c). Here we observe the two sets of Fourier peaks whose translation axes intersect at 60°, i.e., the angle arising from the (111) surface symmetry of diamond microcrystal, and strongly indicating the presence of two spatial periodicities. Surprisingly, the absolute ratio of these spatial periodicities is extremely close to the prime number ratio 2/3. The model "unit cell", which corresponds to the STM data, is shown in the Fig. 2(d). The base and the height of diamond parallelograms, whose exact values have been determined both from Fig. 2(c) and from the high-resolution STM images to be discussed later, are 8.3 and 10.5 nm, respectively. From the cross section of the STM image [see Fig. 2(e)] we determined that the topographic contrast is 15 Å. This is by an order of magnitude larger than the STM contrast typically induced by purely electronic effects. Indeed, as it was shown in earlier STM studies [3,6,28], the vertical contrast due to spatial modulation of electronic density of states is usually $\approx$1 Å. Thus, we have strong reasons to believe that the top surface of *B*-doped diamond microcrystals is comprised of spatially ordered magic-sized diamond grains. Because the grains are very closely spaced their true "height" is likely to be >15 Å [29]. The periodic superstructures, as shown in Figs. 2(a) and 2(b), can be observed by STM on all *B*-doped diamond microcrystals. In some cases we also observed the formation of antiphase twinning boundaries inside of these superstructures. The example of such antiphase boundary is shown in the STM image in Fig. 2(f).

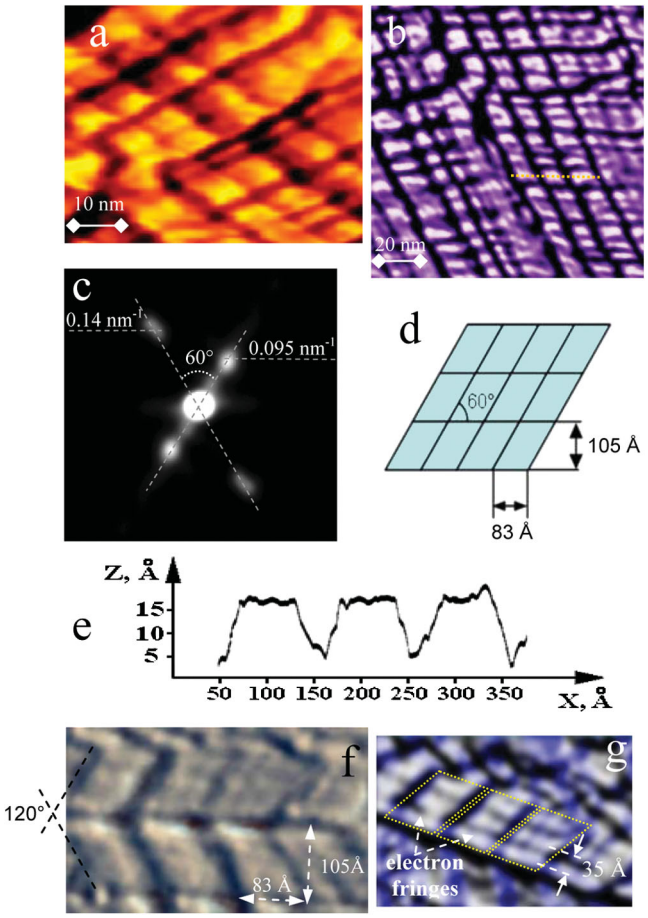

FIG. 2 (color). (a),(b) STM images obtained on top of individual boron-doped diamond microcrystals. The image sizes are (a) 620×500 Å^2 and (b) 1300×1300 Å^2. The measurements were performed at room temperature, using $I = 0.1$ nA and $V = 700$ mV. (c) The 2D Fourier transform of STM image in Fig. 2a. (d) Model two-dimensional array of parallelogram-shaped diamond nanocrystals. The heights of these parallelograms are $L_1 = 83$ Å cos30° $= 72$ Å and $L_2 = 105$ Å, and their ratio is extremely close to the ratio of integers: L_1: $L_2 \approx 2/3$. (e) The cross section of STM image in Fig. 2(b) [see the yellow line across Fig. 2(b)]. (f) 400×240 Å^2 STM image of antiphase boundary of nanoscale diamond grains. The image was obtained at $I = 0.1$ nA and $V = 700$ mV. (g) STM image of "triplet" electronic fringes on top of diamond nanocrystals. The measurements were performed at $I = 0.1$ nA and $V = 500$ mV.

One can see two mirrorlike oriented stripes of periodically ordered parallelogram-shaped diamond nanocrystals. This STM image additionally confirms the lateral dimensions of diamond nanocrystals that were previously shown in Fig. 2(d). In addition to the structure-induced STM contrast, visible in the cross section in Fig. 2(e), on top surfaces of diamond nanocrystals STM also resolved fine triplet structure of 35-Å-spaced fringes. These fringes are shown in Fig. 2(g). The vertical contrast of these fringes $\approx$1 Å strongly suggests their purely electronic rather than structural origin. As it will be discussed later in more

detail, the superstructure of magic-sized diamond nanoparticles arises from dopant-induced quantum effects, and the lateral fringes inside these nanoparticles reflect the development of lateral standing electron waves: the driving force of the electronic growth mechanism.

For comparison, in Fig. 3(a) we show the typical STM image of boron-free nanocrystalline diamond film. This sample was prepared under similar conditions, although without B doping. Because of lack of room-temperature electrical conductivity in this sample, the STM measurements were performed at 420 °C. We observed 10–20 nm diamond grains whose distribution of shapes and sizes is quite random, resulting in disordered polycrystalline film morphology. The absence of spatial order in this sample is also confirmed in the 2D STM Fourier transform shown in Fig. 3(b). Very similar film morphologies of pure nanocrystalline diamond had been reported in the earlier AFM studies [30].

Although the growth of pure nanocrystalline diamond films, shown in Fig. 3(a), had been known before [17,30], and their imaging has been done in our study for comparison purposes only, the growth of oriented boron-rich nanocrystals with uniform size distribution, as in Fig. 2, represents new and previously unknown phenomenon. Apparently, only the physical mechanism imposing strict geometrical selection rules for growth of nanocrystals can be

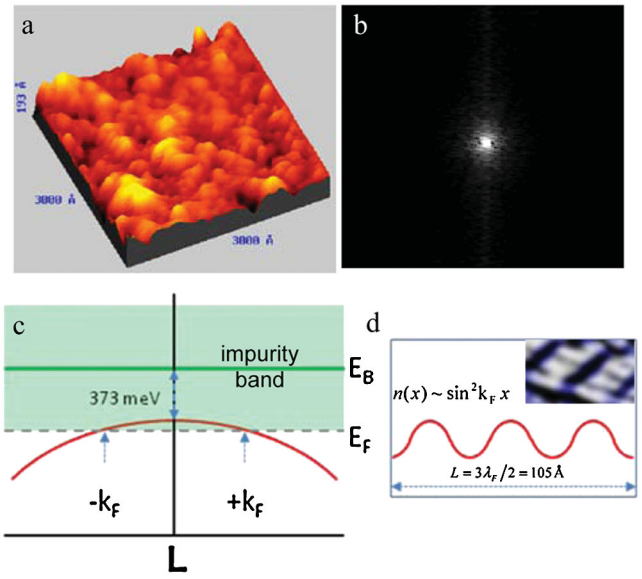

FIG. 3 (color). (a) Typical STM image of undoped nanocrystalline diamond film. The image sizes are 3000×3000 Å^2. The measurements were made at 420 °C using $I = 0.1$ nA and $V = 1500$ mV. (b) The 2D Fourier transform of STM image in (a). (c) The energy diagram illustrating the development of the Fermi sea in heavily doped diamond. This bulk energy diagram remains essentially valid for individual nanocrystals shown in Fig. 2 due to large ($>10^2$) number of boron atoms contained in each of them. (d) The oscillations of electron density in $3\lambda_F/2$ quantum dot. Inset: the fragment of STM image from Fig. 2(g).

responsible for this phenomenon. We believe that the observation of fine triplet structure of electron fringes on top of B-doped nanocrystals provides insight into the possible nature of these geometrical selection rules. As it was shown in the earlier published experimental and theoretical studies of metallic nanostructures [1,2,4–6,10], the magic sizes can develop due to quantum size-effect. According to this electronic growth mechanism, as long as the size of the nanostructure remains less than

$$L_N = \frac{N\lambda_F}{2}, \tag{1}$$

with λ_F being the Fermi wavelength and $N = 1, 2, 3, \ldots$, the time evolution of its growth remains extremely fast. Upon reaching this magic size, i.e., when the corresponding quantum-dot-shell is fully developed, the time evolution of growth slows down by orders of magnitude. This happens due to the oscillatory size dependence of the energy of nanostructures. As a consequence, at any given time the observed size distribution of nanostructures exhibits strong maxima at the discrete values predicted by Eq. (1). Thus, according to earlier studies, the quantum size-effect can impose strict geometrical selection rules for growth of nanoparticles. In semiconductors, the realization of such electronic growth requires extremely high levels of doping leading to the insulator-to-metal transition and the development of the Fermi sea, i.e., exactly what takes place in B-doped diamond. Assuming the 35-Å spacing between the lateral electronic fringes observed by STM on top of diamond nanoparticles to be $1/2\lambda_F$, [31–35] which represents the spatial periodicity of Friedel oscillations, and taking into account the well-known relation between this length scale and the concentration of free carriers [36]

$$\frac{\lambda_F}{2} = \left(\frac{3n_c}{\pi}\right)^{-1/3}, \tag{2}$$

we are coming to the conclusion that at the surfaces of studied B-doped samples $n_c = 2.44 \times 10^{19}$ cm^{-3}. On the other hand, as it was shown in the earlier published transport studies of B-doped diamond films, in the heavily doped regime the portion of ionized boron impurities is $\sim 10^{-2}$ at room temperature [12]. This happens because of the development of broad impurity band, which significantly reduces the effective activation energy of boron dopants. Therefore, the concentration of boron atoms in diamond nanoparticles in Fig. 2 can be estimated as 10^{21} cm^{-3}, which is (a) well above the boron density required for insulator-to-metal transition [11–14], and (b) by an order of magnitude larger than the nominal bulk concentration. Indeed, boron atoms have been known for their tendency to segregate at semiconductor surfaces [37]. Thus, the superstructures on surfaces of studied B-doped diamond samples are most likely caused by the insulator-to-metal transition at extremely high concentration of dopant (10^4 ppm). As we speculate in Figs. 3(c) and 3(d),

under these conditions the boron impurity band considerably broadens and overlaps the diamond valence band edge [15], which causes the system to behave as a degenerate metal with $k_F \approx 0.089$ Å^{-1}. In this metallic regime, which in our samples develops primarily at the surface, the geometries of individual nanoparticles become strongly affected by dopant-induced electronic growth mechanism with the quantum magic size $L = 3\lambda_F/2$. The number of 2D metallic holes per each diamond nanocrystal equals to (island area) $\times\, n_c^{2/3} \approx 7$. In Fig. 3(d) we show the lateral profile of electron density oscillations in $3\lambda_F/2$ quantum dot, which consists of three $\lambda_F/2$—separated density maxima, similar to the triplet structure of electron fringes observed by STM. For simplicity, only the Fermi level contribution has been taken into account in Fig. 3(d). The additional fact strongly indicating in favor of our model is that the height-ratio of diamond parallelograms, which essentially represents the ratio of two spatial periodicities [see Figs. 2(c), 2(d), and 2(f)], is extremely close to the ratio of integers, i.e., 72 Å: 105 Å $\approx 2/3$, as indeed anticipated for the 2D electronic growth according to Eq. (1). Although the quantum size-effect can quantitatively justify the experimentally observed spatial periodicities: $L_1 = \lambda_F$ and $L_2 = 3\lambda_F/2$, it cannot explain why the 2/3-ratio yields the stable energy minima responsible for growth of ordered nanocrystals. Unlike in thin films, where electronic growth had been mostly studied, in quantum dots there exist additional factors which can contribute to the energy balance, such as: the number of filled electronic shells (including the parity effect) and the interdot coupling. These factors, extremely sensitive to the island area, in combination with the quantum size-effect can be responsible for detailed structure of diamond superlattice.

The STM study of magic-sized nanocrystals on surface of boron-doped metallic diamond, described in this Letter, clearly demonstrates that the interplay of structural and electronic properties of materials greatly enhances at nanometer scale and in reduced dimensions. We showed that the crucial role in this process belongs to the competition between classical and quantum effects.

The authors acknowledge N. Zhitenev, L. Bartels, J. A. Carlisle, E. I. Altman, D. M. Chen, and Z. Zhang for interesting discussions. We gratefully acknowledge N. Kane the president of Advanced Diamond Technologies, Inc. for giving us precommercial samples of boron-doped diamond films. This work was supported by the Extreme Friction MURI program, AFOSR Grant No. FA9550-04-1-0381.

[1] Z. Zhang, Q. Niu, and C. K. Shih, Phys. Rev. Lett. **80**, 5381 (1998).
[2] M. Hupalo and M. C. Tringides, Phys. Rev. B **65**, 115406 (2002).
[3] I. B. Altfeder, K. A. Matveev, and D. M. Chen, Phys. Rev. Lett. **78**, 2815 (1997).
[4] J. Chen *et al.*, Phys. Rev. B **77**, 233302 (2008).
[5] S. H. Chang *et al.*, Phys. Rev. B **65**, 245401 (2002).
[6] I. B. Altfeder *et al.*, Phys. Rev. Lett. **92**, 226404 (2004).
[7] H. Okamoto, D. M. Chen, and T. Yamada, Phys. Rev. Lett. **89**, 256101 (2002).
[8] R. M. Feenstra and M. A. Lutz, Phys. Rev. B **42**, 5391 (1990).
[9] J. L. Li *et al.*, Phys. Rev. Lett. **88**, 066101 (2002).
[10] G. Pawin, K. L. Wong, K. Y. Kwon, and L. Bartels, Science **313**, 961 (2006).
[11] V. Mortet *et al.*, Diam. Relat. Mater. **17**, 1330 (2008).
[12] E. Bustarret *et al.*, Phys. Rev. Lett. **93**, 237005 (2004).
[13] Z. L. Wang *et al.*, Diam. Relat. Mater. **15**, 659 (2006).
[14] E. A. Ekimov *et al.*, Nature (London) **428**, 542 (2004).
[15] K.-W. Lee and W. E. Pickett, Phys. Rev. Lett. **93**, 237003 (2004).
[16] I. S. Beloborodov *et al.*, Phys. Rev. B **74**, 235434 (2006).
[17] D. M. Gruen, Annu. Rev. Mater. Sci. **29**, 211 (1999).
[18] S. Bhattacharyya *et al.*, Appl. Phys. Lett. **79**, 1441 (2001).
[19] J. E. Butler and A. V. Sumant, Chem. Vapor Dep. **14**, 145 (2008).
[20] O. A. Williams *et al.*, Diam. Relat. Mater. **17**, 1080 (2008).
[21] J. Mort *et al.*, Appl. Phys. Lett. **55**, 1121 (1989).
[22] R. E. Stallcup *et al.*, J. Vac. Sci. Technol. B **14**, 929 (1996).
[23] Y. D. Kim *et al.*, Diam. Relat. Mater. **9**, 1096 (2000).
[24] T. Nishizaki *et al.*, J. Phys. Chem. Solids **69**, 3027 (2008).
[25] A. Troyanovskiy, T. Nishizaki, and E. Ekimov, Sci. Tech. Adv. Mater. **7**, S27 (2006).
[26] J. W. Steeds *et al.*, Mater. Chem. Phys. **81**, 281 (2003).
[27] S. J. Charles *et al.*, Mater. Lett. **57**, 3690 (2003).
[28] I. B. Altfeder, D. M. Chen, and K. A. Matveev, Phys. Rev. Lett. **80**, 4895 (1998).
[29] The real heights of diamond nanocrystals must be sufficiently large (3–4 nm) for development of 2D electron gas.
[30] N. N. Naguib *et al.*, Chem. Phys. Lett. **430**, 345 (2006)
[31] M. F. Crommie, C. P. Lutz, and D. M. Eigler, Nature (London) **363**, 524 (1993).
[32] I. Brihuega *et al.*, Phys. Rev. B **69**, 155407 (2004).
[33] J. Kliewer and R. Berndt, Phys. Rev. B **65**, 035412 (2001).
[34] H. Yamaguchi *et al.*, Physica (Amsterdam) **E23**, 285 (2004).
[35] W. B. Jian *et al.*, Phys. Rev. Lett. **90**, 196603 (2003).
[36] Ch. Kittel, *Introduction to Solid State Physics* (John Wiley & Sons, New York, 2004), 8th ed.
[37] F. Thibaudau *et al.*, Europhys. Lett. **25**, 353 (1994).